Arbitrary relaxation rate under non-Hermitian matrix iterations

Jaš Bensa
Department of Physics, Faculty of Mathematics and Physics, University of Ljubljana, 1000 Ljubljana, Slovenia

(Received 26 January 2024; accepted 11 June 2024; published 28 June 2024)

We study the exponential relaxation of observables propagated with a non-Hermitian transfer matrix, an example being out-of-time-ordered correlations (OTOC) in brick-wall (BW) random quantum circuits. Until a time that scales as the system size, the exponential decay of observables is not usually determined by the second largest eigenvalue of the transfer matrix, as one can naively expect, but it is, in general, slower—this slower decay rate was dubbed "phantom eigenvalue." Generally, this slower decay is given by the largest value in the pseudospectrum of the transfer matrix; however, we show that the decay rate can be an arbitrary value between the second largest eigenvalue and the largest value in the pseudospectrum. This arbitrary decay can be observed, for example, in the propagation of OTOC in periodic boundary conditions BW circuits. To explore this phenomenon, we study a matrix iteration made from a simple tridiagonal Toeplitz matrix. This setting can be used to propagate OTOC in random circuits with open boundary conditions and to describe a one-dimensional biased random walk with dissipation at the edges.

DOI: 10.1103/PhysRevResearch.6.023331

I. INTRODUCTION

Physical phenomena are often considered intriguing because they stand counter to our classical intuition. Quantum mechanics offers a plethora of such phenomena, for example, the uncertainty principle [1] or quantum entanglement [2], which are phenomena that can be considered "spooky" when compared to classical expectations. Even though quantum mechanics is *the* counterintuitive theory, familiarity has been developed for closed systems, which are subject to Hermitian evolution. However, real-life systems are never closed, leading to non-Hermitian propagation, for example, the Lindblad master equation [3]. Non-Hermitian physics is often thought of as counterintuitive even among quantum mechanics itself, and leads to interesting behavior such as the non-Hermitian skin effect [4–19], relaxation in Liouvillian systems [20–24], and phantom eigenvalues [25–30]. In this paper, we delve into the phantom eigenvalue phenomenon, which appears in the decay of observables propagated using a non-Hermitian transfer matrix.

Observables $O(t)$ which are propagated using a transfer matrix tend to decay towards their asymptotic value $O(\infty)$ exponentially,

$$O(t) - O(\infty) \propto \lambda_{\text{eff}}^{t}(t). \tag{1}$$

In recent work [26,31–34], it was shown that purity and out-of-time-ordered correlations (OTOC) [35–37] in random circuits can be propagated using a transfer matrix approach. It was noted that these quantities exhibit a two-stage exponential relaxation towards their asymptotic values [25,26], namely,

$$\lambda_{\text{eff}}(t) = \begin{cases} \lambda_{\text{ph}}, & t \lesssim n \\ \lambda_2, & t \gtrsim n, \end{cases} \tag{2}$$

where λ_2 is the second largest eigenvalue of the transfer matrix (the largest is equal to 1 and corresponds to the stationary state). Note that the initial decay λ_{ph} persists until extensive times in the system size, meaning that the effective decay $\lambda_{\text{ph}} \neq \lambda_2$ will be present for all times in the thermodynamic limit. This behavior was dubbed phantom eigenvalue in previous papers [25].

Typically, the decay λ_{ph} in processes involving a non-Hermitian transfer matrix is determined by the largest eigenvalue of the slightly perturbed transfer matrix [27,28], i.e., the largest value λ_{ps} in the pseudospectrum [38,39]. In this paper, we instead observe that the decay can be an arbitrary value between λ_2 and λ_{ps}. This happens, for example, in the OTOC relaxation in a brick-wall (BW) periodic boundary conditions (PBC) random quantum circuit; see Fig. 1 for a schematic representation of the circuit. We work out the details behind this arbitrary relaxation and find that surprisingly, the behavior is not determined exclusively by the properties of the transfer matrix but depends on the specifics of the initial vectors used in the iteration.

Such a decay will be observed by examining the behavior of OTOC in a chain of $2n$ qudits of dimension q,

$$O(t) = 1 - \tfrac{1}{2^{2n}}\text{tr}[X_i(t)Y_jX_i(t)Y_j], \tag{3}$$

where X_i and Y_j are two local Pauli-like matrices located at qudit i and j, respectively. Note that $O(t)$ depends on both i and j, but we will leave the dependence implicit. The matrix X_i is propagated in time with a random quantum circuit U of depth t ($2t$ rows of a BW geometry), namely, $X_i(t) = U^\dagger X_i U$. The random matrix U is composed of two-site independent Haar unitaries, which are multiplied in a brick-wall manner

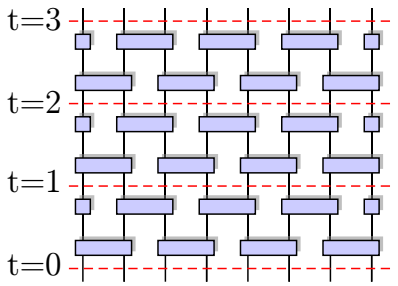

FIG. 1. Schematic representation of a brick-wall (BW) circuit. Blue gates denote two-site Haar random unitaries that act on neighboring qudit pairs (vertical wires). The pattern of gates is periodic and each period of the circuit corresponds to a unit of time.

(Fig. 1). Because the unitaries in the circuit are random, $O(t)$ is independent of the choice of the matrices X and Y.

First, we will look into PBC random quantum circuits. Specifically, we will derive a transfer matrix propagation approach to study the OTOC. Consequently, we will observe an intriguing behavior in its decay towards its asymptotic value. Remarkably, the decay in the thermodynamic limit (TDL) is neither given by the second largest eigenvalue of a transfer matrix, nor by the pseudospectrum, but

$$\lambda_2 < \lambda_{\rm ph} < \lambda_{\rm ps}. \tag{4}$$

See Fig. 2 for a graphic representation.

To understand this phenomenon better, we will delve into the simpler case of OTOC in BW open boundary condition (OBC) circuits (in the circuit from Fig. 1, we do not act with the gate that connects the first and last qubits). In this case, OTOC is propagated with a simple tridiagonal Toeplitz transfer matrix. The simplicity of the matrix will allow for a deeper understanding of the arbitrary relaxation. Namely, focusing on general iterations of this transfer matrix, we will explain why $\lambda_{\rm ph}$ can be a value between λ_2 and $\lambda_{\rm ps}$. As a side remark, we will find that the transfer matrix used to describe OTOC dynamics can also be used to describe other processes, such as a biased one-dimensional (1D) random walk with dissipation at the edges; see Appendix B 3. This

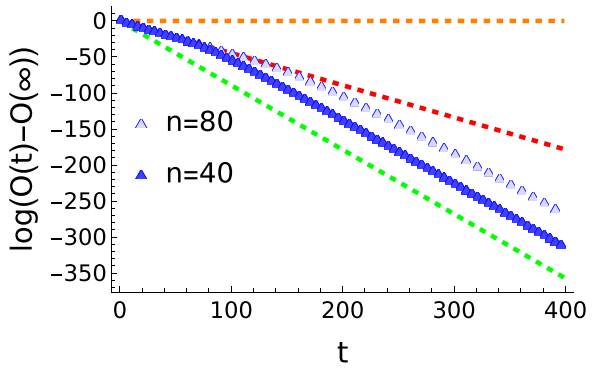

FIG. 2. OTOC in BW PBC circuit initially decays as $\lambda_{\rm ph} = (4/5)^2$ (red slope), which is between $\lambda_2 = (4/5)^4$ (green slope) and $\lambda_{\rm ps} = 1$ (red slope). With increasing system size, the transition point from $\lambda_{\rm ph}$ to λ_2 grows linearly, making the decay $\lambda_{\rm ph}$ the true decay of OTOC in the TDL.

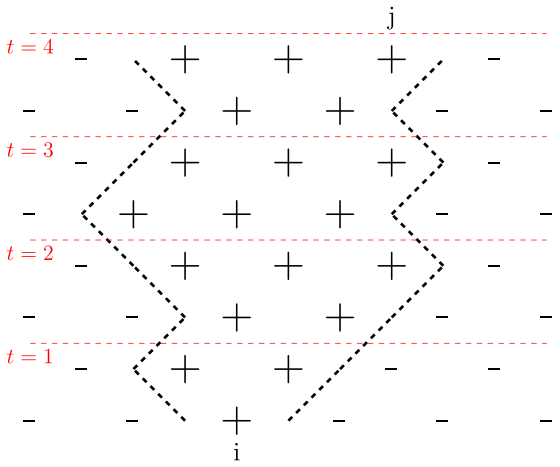

FIG. 3. Schematic representation of a domain that contributes to the partition function for $O_{i,j}(t = 4)$. The domain starts around the site of the initial Pauli-like matrix i and contains the site j at time $t = 4$.

equivalence hints that phantom eigenvalues might be found in more diverse systems besides purity and OTOC evolutions in random quantum circuits. In Appendix B 3, we leverage the equivalence between OTOC dynamics and a biased random walk to obtain a closed-form solution for $O(t)$ in semi-infinite systems.

II. PERIODIC BOUNDARY CONDITIONS

The average time evolution of OTOC in BW PBC circuits is equivalent to a partition function of an Ising-like model [40]. Namely, the authors of Ref. [40] showed that after averaging over all the two-site random unitaries in the circuit, $O(t)$ becomes a partition function of a grid of Ising spins with dimensions $n \times 2t$, which is tilted by 45 degrees; see Fig. 3. The grid is obtained by replacing all the two-site unitaries with two-level spins, $s \in \{+, -\}$. To obtain $O(t)$, one must sum over all 2D domains that start on the qudit i and contain the qudit j at time t; see Fig. 3.

Each domain has its own weight, which is determined by the number of $+$ spins on the top edge of the grid and by the length of the domain walls. For each $+$ in the top edge, we multiply the weight of the domain by q^2. Each opposite horizontally neighboring spin (except on the bottom edge) contributes with $q/(q^2+1)$. For the example in Fig. 3, the weight of the domain is $(q^2)^3(\frac{q}{q^2+1})^{14}$ because the domain has 3 qudits in the top edge and 14 differently oriented neighboring spins (bottom edge excluded). In an infinite system, the number of differently oriented neighboring spins is equal to $4t$, but in a finite system, it could be smaller if the domain hits the boundary of the system or if, at some point in time, the $+$ spin spans over all sites. Namely, the computation of partition functions of the 2D grid of Ising spins works well for infinite systems [40], but gives complicated solutions expressed with recursion for finite systems [26].

To summarize, OTOC in BW circuits can be expressed as a weighted sum of domains on a 2D grid that start at qudit i and contain the qudit j in the top edge. In this paper,

however, instead of looking at the partition function of a 2D grid, as the authors of [40] did, we will compute OTOC by evolving all possible domains of the 1D Ising chain, obtained by considering the vertical axis of the 2D grid as time. To obtain $O(t)$, we then just sum the weight of relevant domains at time t. These weights can now be thought of as probabilities in this Markovian propagation. This Markovian propagation of domain wall to compute OTOC is preferable when dealing with finite systems because it is easy to take into account the boundaries of the system. Using the Markovian propagation of domain weights, in Appendix B 3, we see that we can obtain a simpler closed-form solution of OTOC in semi-infinite circuits.

Now, we shall derive the Markovian evolution of OTOC in PBC by composing a transfer matrix that propagates all domains in the previously mentioned 1D Ising chain [41]. To begin, we shall encode all domains in the vector $|v\rangle$ such that the domain beginning at the i_zth spin and having width $w \in \{1, \ldots, n-1\}$ is written in the $ni_z + w$ component of $|v\rangle$. Note that n counts the number of spins, which is half of the number of qudits. The only domain of width n will be put in the last position of $|v\rangle$, so $|v\rangle$ will be a vector of $n(n-1)+1$ components.

To propagate $|v\rangle$ in time, we can construct a transfer matrix that propagates all domains of the 1D chain of Ising spins. The rules on how to obtain the transfer matrix are explained above. For the sake of simplicity, we will omit these calculations and state the result. We get

$$A = \begin{pmatrix} \mathrm{T} & 0 \\ b & 1 \end{pmatrix}, \tag{5}$$

where T is a block circulant matrix,

$$T = \begin{pmatrix} C & U & 0 & \ldots & D \\ D & C & U & \ldots & 0 \\ \vdots & \ddots & \ddots & \ddots & \vdots \\ 0 & \ldots & D & C & U \\ U & \ldots & 0 & D & C \end{pmatrix}. \tag{6}$$

The vector b describes the transition probabilities to the steady state, i.e., a 1D chain of Ising spins with all $+$. C dictates how the domain width changes for fixed i_z. U and D describe how to obtain domains with $i_z - 1$ or $i_z + 1$ from i_z, respectively. The matrices D, U, and C are tridiagonal matrices because of locality in the random walk of domain width and have dimension $(n-1) \times (n-1)$. T has a block circulant form because of the locality in the changes in i_z. These matrices are

$$C = \begin{pmatrix} 3\tau\sigma & \delta\tau & 0 & \ldots & 0 \\ \delta\sigma & 4\tau\sigma & \delta\tau & \ldots & 0 \\ \vdots & \ddots & \ddots & \ddots & \vdots \\ 0 & \ldots & \delta\sigma & 4\tau\sigma & \delta\tau \\ 0 & \ldots & 0 & \delta\sigma & 3\tau\sigma \end{pmatrix}, \tag{7}$$

$$D = \begin{pmatrix} \tau\sigma & \delta\tau & \tau^2 & 0 & \ldots & 0 \\ 0 & \tau\sigma & \delta\tau & \tau^2 & \ldots & 0 \\ \vdots & \ddots & \ddots & \ddots & \ddots & \\ 0 & \ldots & 0 & \tau\sigma & \delta\tau & \tau^2 \\ 0 & \ldots & 0 & 0 & \tau\sigma & \delta\tau \\ 0 & \ldots & 0 & 0 & 0 & \tau\sigma \end{pmatrix}, \tag{8}$$

$$U = \begin{pmatrix} \tau\sigma & 0 & 0 & 0 & \ldots & 0 \\ \delta\sigma & \tau\sigma & 0 & 0 & \ldots & 0 \\ \sigma^2 & \delta\sigma & \tau\sigma & 0 & \ldots & 0 \\ \vdots & \ddots & \ddots & \ddots & \ddots & \\ 0 & \ldots & \sigma^2 & \delta\sigma & \tau\sigma & 0 \\ 0 & \ldots & 0 & \sigma^2 & \delta\sigma & \tau\sigma \end{pmatrix}, \tag{9}$$

where $\delta = \frac{2q^2}{(1+q^2)^2}$, $\tau = \frac{1}{(1+q^2)^2}$, and $\sigma = \frac{q^4}{(1+q^2)^2}$. Each diagonal in C, D, and U links domains with different widths: the main diagonal connects domains with the same width, the upper diagonal connects domains with width w at time t with the domains of width $w+1$ at time $t-1$, and so on. A row of T is thus composed of n blocks with size $(n-1) \times (n-1)$. The last row b of A is a vector of $n(n-1)$ components. The nonzero components of b are $b_{(n-1)i-1} = \sigma^2$ and $b_{(n-1)i} = \delta\sigma + q^2\sigma$ for $i \in \{1, \ldots, n\}$. These components link the stationary state domain that spans the whole system with domains with smaller widths.

We shall always begin with the initial vector $|v\rangle$ located on the last spin. This choice is irrelevant because of the periodic boundary conditions. The vector $|v\rangle$ is obtained by propagating the domain on the last site for a half-time step. The only nonzero components of $|v\rangle$ are $v_1 = q^2$, $v_{(n-1)^2+1} = q^2$, and $v_{(n-1)^2} = q^4$. On the other hand, we must be careful when we choose $\langle p|$. Depending on the position of the qudit j, the nonzero components are $p_{(n-1)(i-1)+k} = 1$ for $i \in \{1, \ldots, n\}$ and $k \in \{j - i + 1 \mod n - 1, \ldots, n-1\}$ and $p_{n(n-1)+1} = 1$.

To calculate the average OTOC at time t, we iterate the transfer matrix A on the initial vector $|v\rangle$ t times, $t \in \mathbb{N}$. By doing so, we propagate all domains that span from our initial domain until time t. The domains relevant for the partition function from [40] are extracted by projecting $A^t|v\rangle$ on the vector $\langle p|$,

$$O(t) = \langle p|A^t|v\rangle. \tag{10}$$

Once we obtain a transfer matrix approach for computing OTOC, we can compare the actual exponential decay with the second largest eigenvalue λ_2 and the largest pseudoeigenvalue λ_{ps} of A. Figure 4 illustrates that the actual decay λ_{ph} of OTOC between qubits n and $j = 1$, $q = 2$, lies between $\lambda_2 = (4/5)^4$ and $\lambda_{\mathrm{ps}} = 1$ (computed in Appendixes A 1 and A 2, respectively). Namely, $\lambda_{\mathrm{ph}} = (4/5)^2$ [42]. Exact results were also computed for general q, namely, $\lambda_2 = 16q^4/(1+q^2)^4$, $\lambda_{\mathrm{ps}} = 1$, and $\lambda_{\mathrm{ph}} = \lambda_{\mathrm{ph}}^2$. This intriguing behavior is retained for all possible choices of q and j. The underlying reason for this behavior can be attributed to the specific selections of $\langle p|$ and $|v\rangle$ that give OTOC evolution. For general or randomly chosen initial vectors, even though it is not physical, the expression $\langle p|A^t|v\rangle$ decays as λ_{ps}^t until $t \sim n$; see Fig. 4(b) for an example.

III. OPEN BOUNDARY CONDITIONS

Let us continue by examining the propagation of OTOC for BW OBC random quantum circuits. Similar to the case of PBC, OTOC can be obtained by evolving all domains on a 1D Ising chain of n sites and summing only the relevant

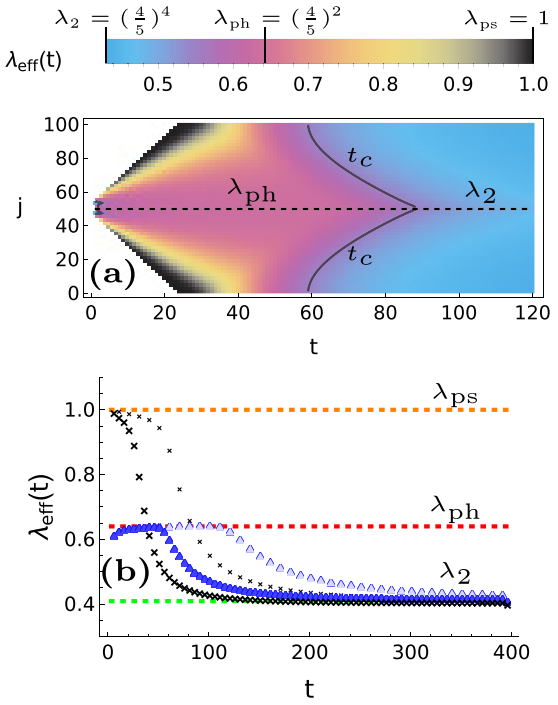

FIG. 4. OTOC time dependence for a BW PBC circuit, $q = 2$. (a) The propagation of $O(t) - O(\infty)$ for different final positions j for $i = n$, $n = 50$. The gray curve denotes the critical time t_c when $\lambda_{\rm eff} = 0.55$. (b) The iteration of A on two different sets of initial vectors: blue symbols denote the choice of vectors that give OTOC dynamics [black dashed line from (a)], black symbols denote the choice of the physical $\langle p|$, but $p_{n(n-1)+1} = 0$, and random v_k, $\sum_k v_k = 1$, that decays as $\lambda_{\rm ps}^t$. The green dotted line denotes the decay given by λ_2, the red dotted line denotes $\lambda_{\rm ph}$, and the orange one denotes the decay for $\lambda_{\rm ps}$. (b) also compares data for $n = 80$ (light symbols) with data for $n = 40$ (dark symbols), which shows that the initial decays persist until $t \sim n$.

domains that are described above. To analyze the correlation between the first ($i = 1$) and the jth qudits, we focus just on the right edge of our domain since the left edge remains fixed at the left boundary of the system. Consequently, at every time, there are only n possible domains, one for each domain width, in contrast to the $\approx n^2$ domains in the PBC scenario. The initial vector $|v\rangle$ must contain the domain on just the first spin. If we order domains by increasing width, we get $v_k = \frac{q^4}{q^4-1}\delta_{1,k}$. This initial vector is propagated with the transfer matrix

$$A = \begin{pmatrix} & \mathrm{T} & & 0 \\ & & & \vdots \\ & & & 0 \\ 0 & \dots & 0 & \sigma & 1 \end{pmatrix};$$

$$T = \begin{pmatrix} \delta & \tau & 0 & \dots & 0 \\ \sigma & \delta & \tau & \dots & 0 \\ \vdots & \ddots & \ddots & \ddots & \vdots \\ 0 & \dots & \sigma & \delta & \tau \\ 0 & \dots & 0 & \sigma & \delta \end{pmatrix}, \tag{11}$$

where $\delta = \frac{2q^2}{(1+q^2)^2}$, $\tau = \frac{1}{(1+q^2)^2}$, and $\sigma = \frac{q^4}{(1+q^2)^2}$. Note that the transfer matrix A exhibits a distinct structure, namely, the first $n-1$ components are propagated using a tridiagonal Toeplitz matrix T [43]. If we are interested in the OTOC between the first qudit and the jth one, the summation over relevant domains is represented with the inner product with the vector $\langle p|$, $p_k = 1$ if $k \geqslant j$ and 0 otherwise, leading to $O(t) = \langle p|A^t|v\rangle$.

In the physical systems that we analyze, the vector $|v\rangle$ is localized at the leftmost position. Thus, for times $t < n$, the iteration with T is equivalent to the iteration with A. Therefore, when we want to analytically study the iteration until extensive times $t \sim n$ (the interesting domain), we can focus on the properties of the iteration $O(t) = \langle p|T^t|v\rangle$. However, note that $O(\infty)$ is still defined as $\lim_{t\to\infty}\langle p|A^t|v\rangle$.

Before moving to the properties for general δ, τ, and σ, we will first examine the classical limit $q \to \infty$. In this case, only $\sigma \neq 0$, so T corresponds to a transposed Jordan kernel. We will generalize this transposed Jordan kernel to a transposed Jordan block with diagonal elements equal to δ (which is zero for $q \to \infty$) and lower diagonal elements σ. Note that the n times degenerate eigenvalue of T is δ and the largest value in the pseudospectrum is $\delta + \sigma$ (Appendix B 1). The physical case $q \to \infty$ is recovered by setting $\delta = 0$ and $\sigma = 1$. When $|v\rangle$ is left-localized, the iteration for times $t < n$ can be expressed as follows:

$$\begin{aligned} O(t) &= \langle p|T^t|v\rangle \\ &= \sum_{r=0}^{\min(t,n-1)} \binom{t}{r} \delta^{t-r}\sigma^r \sum_{j=1}^{n-r} \langle p|e_{j+r}\rangle\langle e_j|v\rangle \\ &= \sum_{r=0}^{\min(t,n-1)} \binom{t}{r} \delta^{t-r}\sigma^r C(r). \end{aligned} \tag{12}$$

The second row is obtained by replacing the tth power of the Jordan block with the tth power of a diagonal matrix of entries δ plus the nilpotent matrix with lower diagonal elements equal to σ. The vectors e_j with kth component $\delta_{j,k}$ are generalized eigenvectors of the nilpotent matrix. The quantity $C(r) = \sum_{j=1}^{n-r}\langle p|e_{j+r}\rangle\langle e_j|v\rangle$ from the last row is the convolution between the initial vectors $\langle p|$ and $|v\rangle$. If $C(r)$ is independent of r, for example, for $p_k = 1$ and $v_k = \delta_{k,1}$, then the sum over r can be evaluated, and $O(t) \propto (\delta + \sigma)^t$ for $t < n$. It is worth noting that $\delta + \sigma$ corresponds to the largest value in the pseudospectrum of T. Interestingly, if $C(r) = \mu^{-r}$, for instance, when $p_k = \mu^{-k}$ and $v_k = \delta_{k,1}$, then $O(t) = (\delta + \sigma/\mu)^t$ for $t < n$. If we want $f(t)$ to be different than 0 in the TDL, we must choose $\mu > 1$. In all the examples, $O(\infty) = 0$, and consequently, the decay of $O(t)$ to its asymptotic value becomes an *arbitrary* number between δ, the largest eigenvalue, and $\delta + \sigma$, the pseudospectrum of T. This brief derivation illustrates that we cannot determine the decay of $O(t)$ solely by examining the properties of the transfer matrix. In the case $C(r) = \mu^{-r}$, the decay depends on the specific form of the initial vectors.

Now, let us move back to the case of general q. The largest value $\lambda_{\rm ps} = \sigma + \delta + \tau = 1$ in the pseudospectrum of T is larger than its largest eigenvalue $\lambda_2 = \delta + 2\sqrt{\sigma\tau}$; see

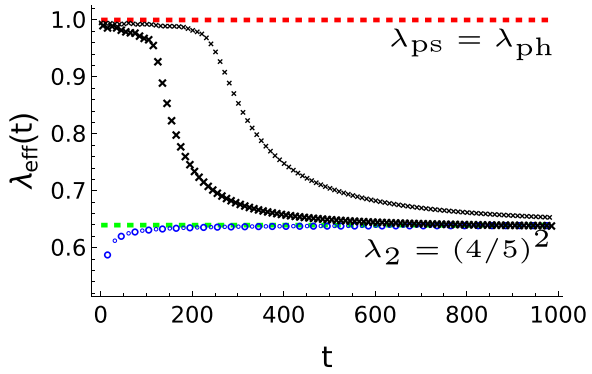

FIG. 5. Iteration of A (OBC, $q = 2$) on two different sets of initial vectors: blue symbols denote the choice of vectors that give OTOC dynamics, black symbols denote the choice $p_k = 1 - \delta_{n,k}$ and random v_k, $\sum_k v_k = 1$, that decays as λ_{ps}^t. The green dotted line denotes λ_2, the red dotted line denotes the value λ_{ps}. The plot also compares data for $n = 80$ (small symbols) with data for $n = 40$ (big symbols), which shows that the initial decays persist until $t \sim n$.

Appendix B 1 for the properties of T. We would expect that quantities such as $O(t) - O(\infty) = \langle p|T^t|v\rangle$ decay as λ_{ps}^t. However, it is known that OTOC decays as λ_2^t [26]. It turns out that the initial vectors for OTOC are special; see Appendix B 2 for a mathematical explanation through an exact computation of $O(t)$. When considering general (or random) $\langle p|$ and $|v\rangle$, the decay of $O(t)$ would indeed be given by the largest value in the pseudospectrum; see Fig. 5.

IV. ARBITRARY DECAY

We have observed that the decay λ_2^t is achieved through the use of special vectors that give OTOC dynamics. Is it possible to get an arbitrary decay rate with an appropriate choice of $\langle p|$ and $|v\rangle$, as we saw for Jordan blocks? Figure 6(a) shows how $O(t) - O(\infty) = \langle p|A^t|v\rangle$ decays for $v_k = \delta_{k,1}$ and $p_k = \mu^{-k}$, $\mu = 1.35$. Although the largest value in the pseudospectrum is 1, this quantity decays as $\approx 0.85^t$, which is between λ_2 and λ_{ps}.

The arbitrary decay can be intuitively understood in terms of the pseudospectrum. Instead of propagating $O(t) = \langle p|T^t|v\rangle$ for $p_k = \mu^{-k}$ and $v_k = \delta_{k,1}$, we instead express it like $\langle \tilde{p}|D^{-1}T^tD|\tilde{v}\rangle$, where $\tilde{p}_k = 1$, so D is a diagonal matrix with diagonal elements $D_{k,k} = \mu^k$. The action of D^{-1} retains the right vector's form, but rescales it. Recall that nonunitary similarity transformations can alter the matrix's pseudospectrum [38]. In fact, the largest value in the pseudospectrum of

$$D^{-1}TD = \begin{pmatrix} \delta & \tau\mu & 0 & \dots & 0 \\ \frac{\sigma}{\mu} & \delta & \tau\mu & \dots & 0 \\ \vdots & \ddots & \ddots & \ddots & \vdots \\ 0 & \dots & \frac{\sigma}{\mu} & \delta & \tau\mu \\ 0 & \dots & 0 & \frac{\sigma}{\mu} & \delta \end{pmatrix} \tag{13}$$

is $\lambda_{ps} = \delta + \frac{\sigma}{\mu} + \tau\mu$, which coincides with the decay of $O(t)$ from Fig. 6(a) for $\mu = 1.35$. A schematic representation of the pseudospectrum of $D^{-1}TD$ for different values μ is shown in

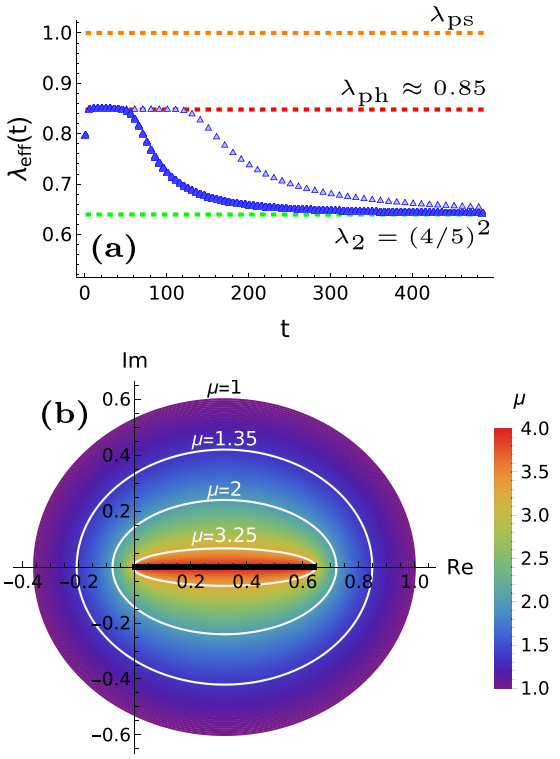

FIG. 6. (a) Iteration of A (OBC, $q = 2$) for $p_k = \mu^{-k}$ and $v_k = \delta_{k,1}$, $\mu = 1.35$. The quantity $\langle p|A^t|v\rangle$ decays towards its asymptotic values as $\lambda_{ph}^t \approx 0.85^t$, and $\lambda_2 < \lambda_{ph} < \lambda_{ps}$. The red line denotes λ_{ph}, the orange line the value $\lambda_{ps} > \lambda_{ph}$, and the green line the asymptotic decay of finite system sizes λ_2. The plot shows data for two system sizes, namely, $n = 80$ for light symbols and $n = 40$ for dark symbols, which shows that λ_{ph} persists until times that are extensive in the system size. (b) Cartoon representation of the pseudospectrum of the matrix from Eq. (13). For different exponential localization μ of the initial vector, we get different pseudospectra. As we increase μ, we get from the pseudospectrum of A for $\mu = 1$ to the spectrum of A for $\mu = 4$. The solid black line on the real axis corresponds to the spectrum of the matrix.

Fig. 6(b). It turns out that λ_{ph} can only be between λ_2 and λ_{ps}. To see this, one can exactly solve all the sums in the expression $O(t) = \langle p|T^t|v\rangle$; see Appendix B 2 for the computation of λ_{ph}. We conclude that the decay of $O(t)$ towards its asymptotic value is not determined solely by the properties of the transfer matrix, but it is highly dependent on the initial vectors used in the iteration.

Note that with Eq. (13), we could get a non-Hermitian matrix from an initially Hermitian matrix ($\sigma = \tau$). Does this mean that a decay slower than λ_2^t is possible in Hermitian systems? We will see that the phantom decay $\lambda_{ph} > \lambda_2$ of quantities $O(t) = \langle p|T^t|v\rangle$ to their asymptotic value $O(\infty)$ is a finite-size effect if T is a symmetric tridiagonal Toeplitz matrix with upper and lower diagonal elements β. Increasing the system size, $O(t)$ approaches 0 for every nonzero time, as seen in Fig. 7. In the TDL, $O(t)$ will be exactly equal to zero for every nonzero time.

To show that phantom relaxations are a finite-size effect in Hermitian systems, let us begin with the initial vectors $p_k \propto \mu^{-k}$ and $v_k = \delta_{k,1}$. The expression $O(t)$ can be

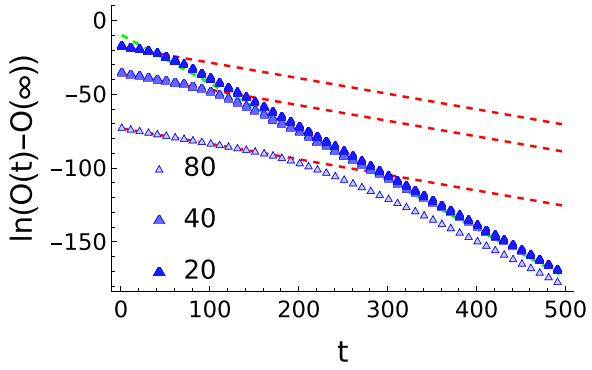

FIG. 7. Iteration of the tridiagonal matrix T with $\delta = 8/25$, $\tau = \sigma = 5/25$ for $p_k \propto \mu^{-k}$ and $v_k = \delta_{k,1}$, $\mu = 0.4$. The vector $\langle p|$ is normalized such that $\sum_k p_k = 1$. The quantity $\langle p|T^t|v\rangle$ decays towards its asymptotic values as $\lambda_{\rm ph}^t \approx 0.85^t$ and $\lambda_2 \approx 0.72$. The red line denotes $\lambda_{\rm ph} \approx 0.85$ and the green line denotes the asymptotic decay of finite system sizes λ_2. Even though the initial decay $\lambda_{\rm ph}$ is larger than λ_2, the plot for different system sizes clearly shows that $O(t = 0)$ approaches 0 by increasing the system size n.

computed using $p_k = 1$ if we appropriately transform T with a similarity transformation, similarly as we did in Eq. (13). In this case, we get an effective iteration with a non-Hermitian matrix, where a decay $\lambda_{\rm ph} > \lambda_2$ should not be surprising. We have

$$D^{-1}TD = \begin{pmatrix} \delta & \beta\mu & 0 & \dots & 0 \\ \frac{\beta}{\mu} & \delta & \beta\mu & \dots & 0 \\ \vdots & \ddots & \ddots & \ddots & \vdots \\ 0 & \dots & \frac{\beta}{\mu} & \delta & \beta\mu \\ 0 & \dots & 0 & \frac{\beta}{\mu} & \delta \end{pmatrix}, \tag{14}$$

where D is a diagonal matrix with diagonal elements equal to $D_{k,k} = \mu^k$. The choice $\mu > 1$ is the only possible choice if we wish to normalize $\langle p|$. In this case, the upper diagonal of $D^{-1}TD$ is larger than its lower diagonal, resulting in a transfer matrix of the same form as the one used to propagate OTOC. Even the initial vectors $p_k = 1$ and $v_k = \delta_{k,1}$ are the same as those used for OTOC, so we know that $O(t)$ will decay to its asymptotic value $O(\infty) = 1$ as λ_2^t.

Another possible choice for $\langle p|$ is when $\mu < 1$. In this case, $\lambda_{\rm ph} > \lambda_2$; however, if we wish to normalize $\langle p|$, then $O(t = 1)$ will scale as $\langle p|v\rangle = \frac{\mu^{-1}}{\sqrt{\sum_k \mu^{-2k}}} \approx \mu^{-n}$. The normalization and right-localization of $\langle p|$ implies that $O(t)$ is exactly zero for every nonzero time in the TDL.

To conclude, we explored the case of Hermitian T and saw that the rate at which $O(t)$ decays to $O(\infty)$ is $\lambda_{\rm ph} > \lambda_2$ only when $\langle p|$ is localized at the right edge of the system, i.e., $\mu < 1$. In this case, however, $O(t)$ decays to 0 for every nonzero time as we increase the system size n, which makes the phantom eigenvalue a finite-size effect in Hermitian systems. In contrast, when T is non-Hermitian, $\lambda_{\rm ph} > \lambda_2$ until extensive times also when $O(t)$ is not zero in the TDL, which makes $\lambda_{\rm ph}$ the only true decay in the TDL.

V. DISCUSSION

We studied the decay of observables $O(t) = \langle p|A^t|v\rangle$ propagated with a non-Hermitian transfer matrix A. Such systems can be found when studying purity or OTOC propagation in random quantum circuits or other Markovian systems. The peculiarity of these systems is that they can exhibit phantom eigenvalues, that is, the convergence of $O(t)$ towards its asymptotic value is not determined by the second largest eigenvalue λ_2 of A, but rather by the largest value $\lambda_{\rm ps}$ in the pseudospectrum of A. In this paper, we have shown that this is not always the case. The exponential rate at which $O(t)$ relaxes can be an arbitrary value between λ_2 and $\lambda_{\rm ps}$. Such "arbitrary" decay happens in physical systems, for example, in OTOC relaxation in PBC BW random quantum circuits. To compute the actual decay rate of $O(t)$, one must not just look at properties of the transfer matrix A, but rather at the whole system. Namely, we found that when $\langle p|$ was exponentially localized, this changed the convergence rate of $O(t)$ to an arbitrary value, which depends on the localization length of $\langle p|$.

Although the decay is not solely determined by the transfer matrix properties, the pseudospectrum still plays a crucial role in the computation of the phantom decay $\lambda_{\rm ph}$. However, it is not the pseudospectrum of the transfer matrix A which we have to explore, but rather the pseudospectrum of the transformed matrix $D^{-1}AD$, where D is chosen so that $\langle p|D$ is exponentially localized. Currently, it is understood that the pseudospectrum of A (or $D^{-1}AD$) determines the exponential relaxation of observables for general initial vectors. However, for special choices of initial vectors, the observable can decay as λ_2. Ultimately, it would be useful to develop a general technique to determine whether an observable decays as $\lambda_{\rm ph} > \lambda_2$ solely from looking at properties of A and initial vectors. This will be ground for future studies.

ACKNOWLEDGMENTS

I would like to thank M. Žnidarič, J. M. Bhat, and K. Kavanagh for valuable discussions and comments on the manuscript. Support from Grants No. P1-0402 and No. J1-4385 from the Slovenian Research Agency is acknowledged.

APPENDIX A: PBC CASE

1. Diagonalization

To diagonalize the transfer matrix A, one can begin by diagonalizing the block circulant matrix T. If λ_k and $|v_k\rangle$ are an eigenpair of T, then λ_k is also an eigenvalue of A whose eigenvector is obtained from $|v_k\rangle$ by adding one last component $\frac{\langle b|v_k\rangle}{\lambda_k - 1}$. There is also an eigenvector of A which is not derived from the eigenvectors of T, namely, $(0, \dots, 0, 1)$ with eigenvalue 1. To diagonalize A, thus one needs first to diagonalize T.

The block circulant matrix can be diagonalized by applying a block Fourier transform $F^\dagger TF$, where F is a matrix of $n \times n$ blocks of size $n-1 \times n-1$. The block at the ith row and jth column of F is a diagonal matrix with constant elements $\exp(2\pi ijk/n)/\sqrt{n}$.

After applying this similarity transformation, we will end up with a block-diagonal matrix with n blocks, where the kth block is

$$T_k = \sigma\tau \begin{pmatrix} 3+d_0 & d_1 & d_2 & 0 & 0 & \dots & 0 \\ d_{-1} & 4+d_0 & d_1 & d_2 & 0 & \dots & 0 \\ d_{-2} & d_{-1} & 4+d_0 & d_1 & d_2 & \dots & 0 \\ & \ddots & \ddots & \ddots & \ddots & \ddots & \\ 0 & \dots & d_{-2} & d_{-1} & 4+d_0 & d_1 & d_2 \\ 0 & \dots & 0 & d_{-2} & d_{-1} & 4+d_0 & d_1 \\ 0 & \dots & 0 & 0 & d_{-2} & d_{-1} & 3+d_0 \end{pmatrix}, \tag{A1}$$

where $d_{-2} = q^4 \exp(2\pi ik/n)$, $d_{-1} = 2q^2[1+\exp(2\pi ik/n)]$, $d_0 = 2\cos(2\pi k/n)$, $d_1 = 2/q[1+\exp(-2\pi ik/n)]$, and $d_2 = 1/q^4 \exp(-2\pi ik/n)$, $k \in \{1,\dots,n\}$. Following [44], we can rewrite the matrix above as a product of two commuting matrices,

$$T_k = \sigma\tau \tilde{A}_k \tilde{B}_k, \quad [\tilde{A}_k, \tilde{B}_k] = 0, \tag{A2}$$

where

$$\tilde{A}_k = \begin{pmatrix} a_1 & b_1 & 0 & \dots & 0 \\ c_1 & a_1 & b_1 & \dots & 0 \\ & \ddots & \ddots & \ddots & \\ 0 & \dots & c_1 & a_1 & b_1 \\ 0 & \dots & 0 & c_1 & a_1 \end{pmatrix}, \tag{A3}$$

$$\tilde{B}_k = \begin{pmatrix} a_2 & b_2 & 0 & \dots & 0 \\ c_2 & a_2 & b_2 & \dots & 0 \\ & \ddots & \ddots & \ddots & \\ 0 & \dots & c_2 & a_2 & b_2 \\ 0 & \dots & 0 & c_2 & a_2 \end{pmatrix}, \tag{A4}$$

where $a_1 = q^2[1+\exp(2\pi ik/n)]$, $b_1 = 1$, $c_1 = q^4 \exp(2\pi ik/n)$, $a_2 = q^{-2}[1+\exp(-2\pi ik/n)]$, $c_2 = 1$, and $b_2 = q^{-4} \exp(-2\pi ik/n)$. The tridiagonal matrices $\tilde{A}_k$ and $\tilde{B}_k$ can be diagonalized simultaneously. The eigenvalues of T are, after simplifications,

$$\lambda_{j,k} = \delta^2 \left[\cos\left(\frac{\pi j}{n}\right) + \cos\left(\frac{\pi k}{n}\right) \right]^2, \tag{A5}$$

where $k \in \{1,\dots,n\}$ is the momentum from the Fourier transformation and $j = \{1,\dots,n-1\}$ runs through the components in the kth Fourier mode. The corresponding left and right eigenvectors $(ln+m)$-th components are

$$[r_{j,k}]_{l\cdot n+m} = \frac{\sqrt{2}q^{2m}}{n} e^{2\pi ikl/n} e^{\pi ikm/n} \sin(jm\pi/n), \tag{A6}$$

$$[l_{j,k}]_{l\cdot n+m} = \frac{\sqrt{2}q^{-2m}}{n} e^{-2\pi ikl/n} e^{-\pi ikm/n} \sin(jm\pi/n), \tag{A7}$$

for $l \in \{1,\dots,n\}$ and $m \in \{1,\dots,n-1\}$.

2. Pseudospectrum

In this Appendix, we shall compute the pseudospectrum of T. The pseudospectrum of a matrix M can be computed numerically via the ϵ-pseudospectrum. The ϵ-pseudospectrum is computed by averaging the spectrum of $M+\epsilon E$ over all matrices E with norm 1. The pseudospectrum of M is then obtained from the ϵ-pseudospectrum by first taking the limit of large system size and then taking $\epsilon \to \infty$. Numerically averaging the spectrum of $M+\epsilon E$ over all E is not possible. Luckily, the ϵ-pseudospectrum can be usually approximated by just one realization of $M+\epsilon E$. Instead of averaging over all E, we will perturb T by a matrix E of norm ϵ and compute its spectrum—we will call this the approximate ϵ-pseudospectrum. If we compute the approximate ϵ-pseudospectrum for a small enough ϵ, after taking the TDL, the resulting set is independent of ϵ. In this case, the pseudospectrum can be computed as the TDL of the approximate ϵ-pseudospectrum, $\epsilon \ll 1$.

In Fig. 8, we plot the approximate ϵ-pseudospectrum for system sizes 80, 120, and 180 and $\epsilon = 10^{-5}$. We choose $\epsilon = 10^{-5}$ because we find that the TDL of the approximate ϵ-pseudospectrum converges fast enough to a set independent of ϵ. The largest value in the approximate ϵ-pseudospectrum approaches 1 as we increase the system size. We conjecture that in the thermodynamic limit, the pseudospectrum T is the union over all values k of the product of the pseudospectra of $\tilde{A}_k$ and $\tilde{B}_k$ from Eq. (A4). This coincides with $(c_1 e^{i\phi} + a_1 + b_1 e^{-i\phi})(c_2 e^{i\phi} + a_2 + b_2 e^{-i\phi})$, for $\phi \in [0, 2\pi]$ and $k/n \in [0, 1]$. The conjectured region is shown in Fig. 8 in black and it seems to match with the plots from Fig. 8 for $n \to \infty$.

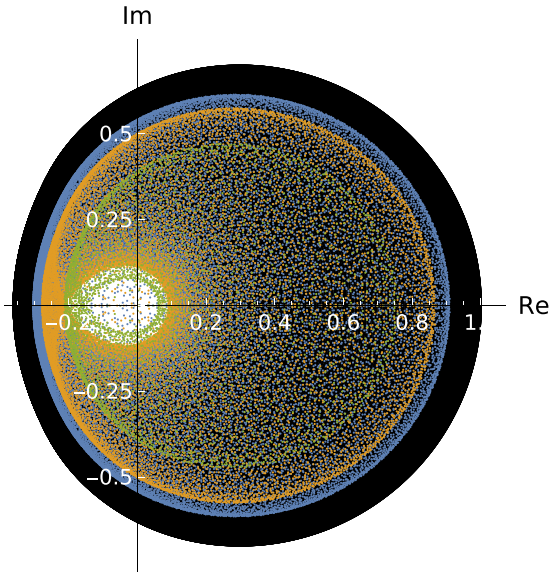

FIG. 8. The colored dots represent the approximate ϵ-pseudospectrum for $n = 80$ (green), $n = 120$ (orange), and $n = 180$ (blue) and $\epsilon = 10^{-5}$. As we increase n, the approximate ϵ-pseudospectrum starts filling the black region, which is our conjecture for the pseudospectrum of T. The black region is obtained as the union of all curves from the conjecture for every possible value of k/n.

APPENDIX B: OBC CASE

1. Transfer matrix properties

Similarly as for the matrix A for PBC, for OBC we can also compute the spectrum of A by first computing the spectrum of the Toeplitz tridiagonal matrix T. Namely, if λ_k and $|v_k\rangle$ are an eigenpair of T, then λ_k is also an eigenvalue of A whose eigenvector is obtained from $|v_k\rangle$ by adding one last component $\frac{\sigma[v_k]_{n-1}}{\lambda_k-1}$. There is also an eigenvector of A which is not derived from the eigenvectors of T, namely, $(0,\ldots,0,1)$ with eigenvalue 1. The eigenvalues of T are [43]

$$\lambda_k = \delta + 2\sqrt{\sigma\tau}\cos\left(\frac{k\pi}{n}\right), \tag{B1}$$

where $k \in \{1,\ldots,n-1\}$. The right eigenvectors $|r_k\rangle$ and left eigenvectors $\langle l_k|$ are

$$[r_k]_j = \left(\frac{\sigma}{\tau}\right)^{j/2}\sin\left(\frac{kj\pi}{n}\right), \tag{B2}$$

$$[l_k]_j = \frac{2}{n}\left(\frac{\tau}{\sigma}\right)^{j/2}\sin\left(\frac{kj\pi}{n}\right). \tag{B3}$$

The pseudospectrum of a Toeplitz matrix T is its symbol $\phi(z)$ evaluated on the unit circle, i.e., the Fourier transformation of its diagonals ($z = e^{i\phi}$) [38]. For our matrix T, we obtain a ϕ-dependent curve given by

$$\delta + e^{i\phi}\tau + e^{-i\phi}\sigma, \quad \phi \in [0, 2\pi]. \tag{B4}$$

Note that the spectrum of T lies on the real values; meanwhile, the pseudospectrum is an ellipse in the complex plane with largest value $\delta+\sigma+\tau$; see Fig. 6(b).

2. Evaluation of $O(t)$ through spectral decomposition of T

In this Appendix, we will evaluate the expression for OTOC,

$$O(t) = \langle p|T^t|v\rangle, \tag{B5}$$

$p_k = 1$ and $v_k = \delta_{k,1}$. As we shall see, the OTOC behaves as $\sim\lambda_{\rm ps}^t = 1$, but if we subtract the steady state of the whole transfer matrix A, the leading term cancels out making $O(t)$ decay as λ_2^t, so we get $O(t) - O(\infty) \asymp \lambda_2^t$, as expected. Even though $O(t)$ does not exhibit phantom behavior, the evaluation of $O(t)$ is interesting because the phantom appears in the solution, but it gets canceled with the steady state that comes from the eigenvalue $\lambda_1 = 1$. This shows that the physical case of OTOC is special because the choice of vectors $\langle p|$ and $|v\rangle$ makes the phantom cancel exactly with $O(\infty)$.

We begin by writing Eq. (B5) with the help of the spectral decomposition of T,

$$O(t) = \frac{2}{n}\sum_{h=1}^{n-1}\lambda_h^t\sqrt{\frac{\sigma}{\tau}}\sin\left(\frac{h\pi}{n}\right)\sum_{k=1}^{n-1}\left(\frac{\sigma}{\tau}\right)^{k/2}\sin\left(\frac{hk\pi}{n}\right), \tag{B6}$$

where $\lambda_h = \delta + 2\sqrt{\sigma\tau}\cos(\frac{h\pi}{n})$. To simplify the expression, we shall first evaluate the sum over the index k. We get

$$\sum_{k=1}^{n-1}\left(\frac{\sigma}{\tau}\right)^{k/2}\sin\left(\frac{hk\pi}{n}\right) = \sqrt{\frac{\sigma}{\tau}}\frac{\left[1-(-1)^h\left(\frac{\sigma}{\tau}\right)^{\frac{n}{2}}\right]\sin\frac{h\pi}{n}}{1+\frac{\sigma}{\tau}-2\sqrt{\frac{\sigma}{\tau}}\cos\frac{h\pi}{n}}. \tag{B7}$$

Plugging Eq. (B7) into Eq. (B6) and rearranging some terms, we get

$$O(t) = \frac{2\tau\left(\frac{\sigma}{\tau}\right)^{\frac{n+1}{2}}}{n}\sum_{h=1}^{n-1}\lambda_h^t\sin^2\left(\frac{h\pi}{n}\right)\frac{\left[\left(\frac{\tau}{\sigma}\right)^{\frac{n}{2}}-(-1)^h\right]}{\lambda_{\rm ps}-\lambda_h}, \tag{B8}$$

where we labeled the largest value in the pseudospectrum $\delta+\sigma+\tau$ with $\lambda_{\rm ps}$. To simplify Eq. (B8), we will assume $\tau<\sigma$ and $n \gg 1$, so that we can neglect the term $(\frac{\tau}{\sigma})^{\frac{n}{2}}$.

We are interested in the time dependence of $O(t)$, so we can forget about the factors outside the sum because they do not contribute to the time dependence of $O(t)$. After these simplifications, we get

$$\sum_{h=1}^{n-1}\lambda_h^t(-1)^h\frac{\sin^2\left(\frac{h\pi}{n}\right)}{\lambda_{\rm ps}-\lambda_h}. \tag{B9}$$

We can replace the fraction $\frac{1}{\lambda_{\rm ps}-\lambda_h}$ with $\frac{1}{\lambda_{\rm ps}}\sum_{r=0}^{\infty}(\frac{\lambda_h}{\lambda_{\rm ps}})^r$ because $\lambda_{\rm ps} > \lambda_h$. Omitting constant terms, we get

$$\begin{aligned}
&\sum_{r=0}^{\infty}\sum_{h=1}^{n-1}\lambda_h^t(-1)^h\sin^2\left(\frac{h\pi}{n}\right)\left(\frac{\lambda_h}{\lambda_{\rm ps}}\right)^r\\
&\quad=\lambda_{\rm ps}^t\sum_{r=0}^{\infty}\sum_{h=1}^{n-1}(-1)^h\sin^2\left(\frac{h\pi}{n}\right)\left(\frac{\lambda_h}{\lambda_{\rm ps}}\right)^{r+t}\\
&\quad=\lambda_{\rm ps}^t\sum_{k=t}^{\infty}\sum_{h=1}^{n-1}(-1)^h\sin^2\left(\frac{h\pi}{n}\right)\left(\frac{\lambda_h}{\lambda_{\rm ps}}\right)^{k}.
\end{aligned} \tag{B10}$$

To prove that $O(t)$ decays as $\lambda_{\rm ps}^t$, we will show that the terms in the sum over the index k are zero for $k \approx n$, meaning that the sum over k runs from $k \approx n$ to ∞ and is independent of t. This, in turn, implies that the only time dependence in the expression (B10) is $\lambda_{\rm ps}^t$.

We continue by summing over the index h,

$$\begin{aligned}
&\sum_{k=t}^{\infty}\lambda_{\rm ps}^{-k}\sum_{h=1}^{n-1}e^{i\pi h}\left(-\frac{1}{4}\right)(e^{i\frac{h\pi}{n}}-e^{-i\frac{h\pi}{n}})^2\\
&\qquad\times(\delta+\sqrt{\sigma\tau}e^{i\frac{h\pi}{n}}+\sqrt{\sigma\tau}e^{-i\frac{h\pi}{n}})^k
\end{aligned} \tag{B11}$$

$$\begin{aligned}
&=\sum_{k=t}^{\infty}\lambda_{\rm ps}^{-k}\sum_{r=0}^{k}\binom{k}{r}\delta^{k-r}(\sigma\tau)^{r/2}\sum_{s=0}^{r}\binom{r}{s}\\
&\qquad\times\sum_{h=1}^{n}[e^{i\frac{h\pi}{n}(2+r-2s+n)}+e^{i\frac{h\pi}{n}(-2+r-2s+n)}-2e^{i\frac{h\pi}{n}(r-2s+n)}]
\end{aligned} \tag{B12}$$

$$\begin{aligned}
&=\sum_{k=t}^{\infty}\lambda_{\rm ps}^{-k}\sum_{r=0}^{k}\binom{k}{r}\delta^{k-r}(\sigma\tau)^{r/2}\\
&\qquad\times\sum_{s=0}^{r}\binom{r}{s}[D_{n-1}(2+r-2s+n)\\
&\qquad+D_{n-1}(-2+r-2s+n)-2D_{n-1}(r-2s+n)],
\end{aligned} \tag{B13}$$

where $D_n(x) = \frac{\sin[(n+1/2)x]}{\sin(x/2)}$ is the Dirichlet kernel [45]. The Dirichlet kernel is composed of a term $(-1)^{x+1}$, which

cancels with the other functions $D_n(x)$ and an infinite series of Kronecker delta functions $\delta_{x/2,\pi p}$, $p \in \mathbb{Z}$. In our case, $x = \frac{r-2s+n+2}{n}$ in the first Dirichlet kernel. The only possible values of p are 0 and 1 because, for other values, there are no s and r to satisfy $x/2 = \pi p$. Moreover, for $p = 0$ and $p = 1$, not all values of r give a nonzero contribution. For example, $x = r - 2s + n + 3$ and $p = 1$ gives $s = (r - n + 1)/2$. The variable s runs from 0 to n, so $(r - n + 1)/2 \geqslant 0$ and $(r - n + 1)/2 \leqslant r$. The former bound gives $r \geqslant n - 1$, the latter $r \geqslant -n$. Computing these bounds for all three Dirichlet kernels and for both $p = 0$ and $p = 1$, we see that $r \gtrsim n$ for each term. This, in turn, implies that the sum over r runs from $\approx n$ to k, so $k \gtrsim n$ to have nonzero contributions. For $k < n$, all terms in the sum over k will be zero, so we can substitute $\sum_{k=t}^{\infty}$ with $\sum_{k\approx n}^{\infty}$, which makes the only time-dependent part of the leading term in $O(t)$ $\lambda_{\rm ps}^t$.

We saw that $O(t)$ behaves as $\lambda_{\rm ps}^t$, but OTOC decay to $O(\infty)$ as λ_2^t. This comes from the fact that the leading term in Eq. (B8) [the one with $(-1)^h$] exactly sums to 1 for $t < n$ (not shown). This means that by subtracting 1 from $O(t)$, we cancel out the leading term of $O(t)$. The subleading term [the neglected term in Eq. (B8)] decays as λ_2^t, and hence OTOC decays as given by the largest eigenvalue of A.

The exact evaluation of $\langle p|T^t|v\rangle$ above can also be used for the case $p_k = \mu^{-k}$. The choice of $\langle p|$ reflects in the evaluation of $\langle p|r_h\rangle$, where $|r_h\rangle$ is an eigenvector of T. We get

$$\langle p|r_k\rangle = \sum_{k=1}^{n-1} \left(\frac{\sigma}{\tau}\right)^{k/2} \mu^{-k} \sin\left(\frac{hk\pi}{n}\right). \tag{B14}$$

Equation (B14) is exactly Eq. (B7) if we substitute τ with $\tau\mu^2$. We can repeat all calculations from before until we get

$$O(t) \propto \sum_{h=1}^{n-1} \lambda_h^t (-1)^h \frac{\sin^2\left(\frac{h\pi}{n+1}\right)}{\lambda(\mu) - \lambda_h}, \tag{B15}$$

with $\lambda(\mu) = \delta + \sigma/\mu + \tau\mu$. Equation (B15) is analogous to Eq. (B9) if we replace $\lambda(\mu)$ with $\lambda_{\rm ps}$. We can repeat all calculations below Eq. (B9) to show that $\lambda(\mu)$ is indeed the true decay of $O(t)$. The value of $\lambda(\mu)$ is greater than λ_2 because otherwise we cannot repeat the steps in Eq. (B10). Moreover, $\lambda(\mu) \leqslant \lambda_{\rm ps} = 1$, otherwise $\langle p|$ is not normalizable. We conclude that $\lambda_2 \leqslant \lambda(\mu) \leqslant \lambda_{\rm ps}$.

3. Biased random walk

In this Appendix, we prove that the OTOC dynamics in a OBC BW circuit is equivalent to a biased 1D random walk coupled to reservoirs at the edges. Using this equivalence, we will be able to compute the decay of OTOC to $O(\infty)$, namely, $O(t) - O(\infty) \asymp \lambda_2^t$, where λ_2 is the second largest eigenvalue of the transfer matrix that propagates OTOC (see Appendix B 1).

The transfer matrix from Eq. (11), used to propagate OTOC, can also be used to describe a 1D biased random walk. To get a proper Markov chain transfer matrix, the elements in each column should sum to 1 to conserve probabilities. To achieve this and keep the tridiagonal transfer matrix to propagate probabilities, one can make the random walk dissipate on the left and right boundary, as shown in Fig. 9. Doing so, the

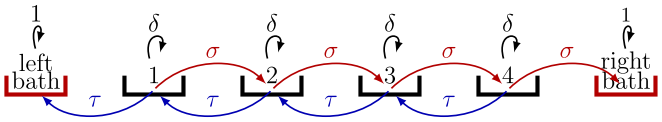

FIG. 9. Cartoon of a biased random walk on four sites with dissipation on the boundary. Above the sites (boxes), possible moves (arrows) with the corresponding probability are shown. Once the random walk enters the reservoirs, it cannot return back to the bulk of the chain.

Markov chain transfer matrix is

$$A = \begin{pmatrix} 1 & \tau & 0 & 0 & 0 & \dots & 0 \\ 0 & \delta & \tau & 0 & 0 & \dots & 0 \\ 0 & \sigma & \delta & \tau & 0 & \dots & 0 \\ \vdots & \vdots & \ddots & \ddots & \ddots & & \vdots \\ 0 & 0 & \dots & \sigma & \delta & \tau & 0 \\ 0 & 0 & \dots & 0 & \sigma & \delta & 0 \\ 0 & 0 & \dots & 0 & 0 & \sigma & 1 \end{pmatrix}, \tag{B16}$$

where $\tau + \sigma + \delta = 1$, and where the first and last sites correspond to the left and right baths, respectively. Note that we could propagate OTOC using this transfer matrix, with $p_k = 1 - \delta_{k,1}$ and $v_k = \delta_{2,k}$. Because $p_1 = 0$, the OTOC can be equivalently propagated by forgetting about the first column and row in Eq. (B16). Using the random walk interpretation, the OTOC $O(t) = \langle p|A^t|v\rangle$ is equivalent to the probability of not being in the left bath by beginning at the second position (left edge of the bulk).

Let us label the probability of being at site j in the bulk with r_{j+1} (so the leftmost site has probability r_2), and the probability of being in the left bath with r_1; then, OTOC is $O(t) = 1 - r_1$. To prove that OTOC decays to its asymptotic value $O(\infty) = 1$ as λ_2^t, we will compute the probability r_1. Because we can enter the left bath just once, the probability r_1 of being in the left bath at time t can be found by summing the probabilities of entering the left bath for all times $T + 1 \leqslant t$. The probability of entering the left bath at time $T + 1$ is obtained as τ times the probability of being at the leftmost site in the bulk 1 at time T without ever being in the left reservoir before. The number of paths of length T beginning at 1 and ending at 1 without going to the left reservoir corresponds to the number of Dyck words [46] with σ and τ. The number of these Dyck words can be expressed with the Catalan number $C_{T/2}$ [47], which is $\binom{T}{T/2}/(T/2+1)$ if T is even and 0 otherwise. The corresponding probability for such a Dyck word is $(\tau\sigma)^{T/2}$. To get the probability of being at 1 at time T without ever being in the left bath, we should also include the moves where we stay at the same place; these moves have probability δ and can be placed anywhere in the Dyck word. To sum up, the probability of being at site 1 at time T is obtained as the sum over all possible combinations of moves to left or right and staying at the same position. At the end, we get

$$r_1(t) = \tau \sum_{T=0}^{t-1} \sum_{k=0}^{T/2} \frac{\binom{2k}{k}}{k+1} (\tau\sigma)^k \delta^{T-2k} \binom{T}{2k}. \tag{B17}$$

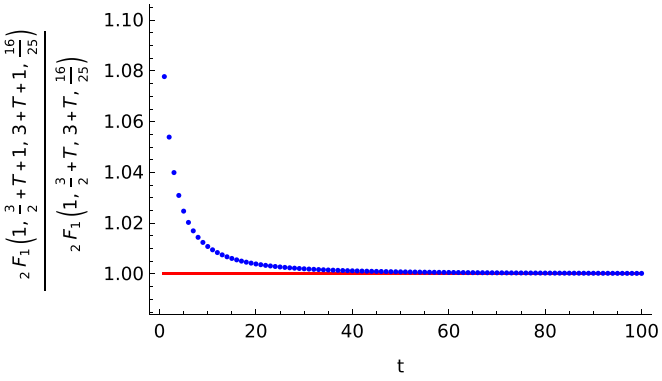

FIG. 10. Ratio of the two hypergeometric functions from Eq. (B19). The ratio decays fast to 1.

OTOC is obtained as $1 - r_1$. For simplicity, we will now compute $O(t)$ for qubits $q = 2$. We get

$$\begin{aligned} O(t) &= 1 - r_1(t) \\ &= 1 + \frac{64}{375\sqrt{\pi}}\left(\frac{16}{25}\right)^t \frac{\Gamma(3/2+t)}{\Gamma(3+t)} \\ &\quad \times {}_2F_1(1, 3/2+t, 3+t, 16/25), \end{aligned} \tag{B18}$$

where ${}_2F_1(a, b, c; z)$ is the hypergeometric function. With the help of the biased random walk picture, in Eq. (B18) we obtained a closed-form solution of OTOC in OBC BW circuits with Haar random two-site gates. A closed-form solution was also obtained in [26], but it is much more complex because it is expressed with recursion. In [40], there is a simple result for OTOC, but it is for infinite systems, whereas our solution holds for any system size n.

Because of the simple form of Eq. (B18), we can compute the rate at which OTOC decays to $O(\infty)$. Assuming OTOC decays to the asymptotic value exponentially, we can get the exponent as $\lambda_{\text{eff}}(t) = \frac{O(t+1)-1}{O(t)-1}$. We get

$$\lambda_{\text{eff}}(t) = \frac{16}{25}\frac{3/2+t}{3+t}\frac{{}_2F_1(1, 5/2+t, 4+t, 16/25)}{{}_2F_1(1, 3/2+t, 3+t, 16/25)}. \tag{B19}$$

The term $\frac{3/2+t}{3+t}$ behaves as $1 - \frac{3}{2t} + O(1/t^2)$, and the ratio of the hypergeometric functions decays to 1 faster than exponentially (Fig. 10), so we conclude that $O(t)$ decays to 1 as $\lambda_{\text{eff}} = 16/25 = \lambda_2$.

We computed the time evolution of a random walk, where we start at the leftmost position in the bulk and we are interested in the probability of staying in the bulk. This random walk coincides with the OTOC evolution in OBC random quantum circuits. When computing the relaxation of OTOC to their asymptotic value $O(\infty)$, we subtract the leading term from $O(t)$, which results in the relaxation given by λ_2. For different initial conditions, subtracting $O(\infty)$ from $O(t)$ does not exactly cancel the leading term in $O(t)$, meaning that $O(t)$ initially does not relax, but stays constant, as we expect by looking at the largest value in the pseudospectrum of the transfer matrix, $\lambda_{\text{ps}} = 1$. OTOC, in this sense, can be considered a special case of initial conditions.

[1] W. Heisenberg, The actual content of quantum theoretical kinematics and mechanics, Z. Phys. **43**, 172 (1927).

[2] A. Einstein, B. Podolsky, and N. Rosen, Can quantum-mechanical description of physical reality be considered complete? Phys. Rev. **47**, 777 (1935).

[3] H.-P. Breuer and F. Petruccione, *The Theory of Open Quantum Systems* (Oxford University Press, 2007).

[4] T. E. Lee, Anomalous edge state in a non-Hermitian lattice, Phys. Rev. Lett. **116**, 133903 (2016).

[5] V. M. M. Alvarez, J. E. B. Vargas, and L. E. F. F. Torres, Non-Hermitian edge states in one dimension: Anomalous localization and eigenspace condensation at exceptional points, Phys. Rev. B **97**, 121401(R) (2018).

[6] S. Yao and Z. Wang, Edge states and topological invariants of non-Hermitian systems, Phys. Rev. Lett. **121**, 086803 (2018).

[7] H. Shen, B. Zhen, and L. Fu, Topological band theory for non-Hermitian Hamiltonians, Phys. Rev. Lett. **120**, 146402 (2018).

[8] F. K. Kunst, E. Edvardsson, J. C. Budich, and E. J. Bergholtz, Biorthogonal bulk-boundary correspondence in non-Hermitian systems, Phys. Rev. Lett. **121**, 026808 (2018).

[9] H. Zhou and J. Y. Lee, Periodic table for topological bands with non-Hermitian symmetries, Phys. Rev. B **99**, 235112 (2019).

[10] K. Kawabata, K. Shiozaki, M. Ueda, and M. Sato, Symmetry and topology in non-Hermitian physics, Phys. Rev. X **9**, 041015 (2019).

[11] L. Li, C.-H. Lee, S. Mu, and J. Gong, Critical non-Hermitian skin effect, Nat. Commun. **11**, 5491 (2020).

[12] D. S. Borgnia, A. J. Kruchkov, and R.-J. Slager, Non-Hermitian boundary modes and topology, Phys. Rev. Lett. **124**, 056802 (2020).

[13] N. Okuma, K. Kawabata, K. Shiozaki, and M. Sato, Topological origin of non-Hermitian skin effects, Phys. Rev. Lett. **124**, 086801 (2020).

[14] K. Zhang, Z. Yang, and C. Fang, Correspondence between winding numbers and skin modes in non-Hermitian systems, Phys. Rev. Lett. **125**, 126402 (2020).

[15] E. J. Bergholtz, J. C. Budich, and F. K. Kunst, Exceptional topology of non-Hermitian systems, Rev. Mod. Phys. **93**, 015005 (2021).

[16] Y. Ashida, Z. Gong, and M. Ueda, Non-Hermitian physics, Adv. Phys. **69**, 249 (2020).

[17] L. E. F. F. Torres, Perspective on topological states of non-Hermitian lattices, J. Phys.: Mater. **3**, 014002 (2020).

[18] N. Okuma and M. Sato, Non-Hermitian topological phenomena: A review, Annu. Rev. Condens. Matter Phys. **14**, 83 (2023).

[19] R. Lin, T. Tai, L. Li, and C. H. Lee, Topological non-Hermitian skin effect, Front. Phys. **18**, 53605 (2023).

[20] F. Song, S. Yao, and Z. Wang, Non-Hermitian skin effect and chiral damping in open quantum systems, Phys. Rev. Lett. **123**, 170401 (2019).

[21] T. Mori and T. Shirai, Resolving a discrepancy between Liouvillian gap and relaxation time in boundary-dissipated quantum many-body systems, Phys. Rev. Lett. **125**, 230604 (2020).

[22] T. Mori, Metastability associated with many-body explosion of eigenmode expansion coefficients, Phys. Rev. Res. **3**, 043137 (2021).
[23] T. Haga, M. Nakagawa, R. Hamazaki, and M. Ueda, Liouvillian skin effect: Slowing down of relaxation processes without gap closing, Phys. Rev. Lett. **127**, 070402 (2021).
[24] T. Mori and T. Shirai, Symmetrized Liouvillian gap in Markovian open quantum systems, Phys. Rev. Lett. **130**, 230404 (2023).
[25] J. Bensa and M. Žnidarič, Fastest local entanglement scrambler, multistage thermalization, and a non-Hermitian phantom, Phys. Rev. X **11**, 031019 (2021).
[26] J. Bensa and M. Žnidarič, Two-step phantom relaxation of out-of-time-ordered correlations in random circuits, Phys. Rev. Res. **4**, 013228 (2022).
[27] M. Žnidarič, Solvable non-Hermitian skin effect in many-body unitary dynamics, Phys. Rev. Res. **4**, 033041 (2022).
[28] J. Bensa and M. Žnidarič, Purity decay rate in random circuits with different configurations of gates, Phys. Rev. A **107**, 022604 (2023).
[29] M. Žnidarič, Phantom relaxation rate of the average purity evolution in random circuits due to Jordan non-Hermitian skin effect and magic sums, Phys. Rev. Res. **5**, 033145 (2023).
[30] C. Jonay and T. Zhou, A physical theory of two-stage thermalization, arXiv:2310.04491 [Phys. Rev. B (to be published)].
[31] W.-T. Kuo, A. A. Akhtar, D. P. Arovas, and Y. Z. You, Markovian entanglement dynamics under locally scrambled quantum evolution, Phys. Rev. B **101**, 224202 (2020).
[32] R. Oliveira, O. C. O. Dahlsten, and M. B. Plenio, Generic entanglement can be generated efficiently, Phys. Rev. Lett. **98**, 130502 (2007).
[33] M. Žnidarič, Exact convergence times for generation of random bipartite entanglement, Phys. Rev. A **78**, 032324 (2008).
[34] A. Nahum, J. Ruhman, S. Vijay, and J. Haah, Quantum entanglement growth under random unitary dynamics, Phys. Rev. X **7**, 031016 (2017).
[35] N. Lashkari, D. Stanford, M. Hastings, T. Osbornee, and P. Hayden, Towards the fast scrambling conjecture, J. High Energ. Phys. 04 (2013) 022.
[36] S. H. Shenker and D. Stanford, Multiple shocks, J. High Energ. Phys. 12 (2014) 46.
[37] J. Maldacena, S. H. Shenker, and D. Stanford, A bound on chaos, J. High Energ. Phys. 08 (2016) 106.
[38] L. N. Trefethen and M. Embree, *Spectra and Pseudospectra* (Princeton University Press, 2005).
[39] If we wish to compute the pseudospectrum numerically, we first compute the spectrum of the slightly perturbed matrix and then take the TDL (see Appendix A 2 for more details). The pseudospectrum can be computed analytically when the matrix is a Toeplitz matrix. In this case, the pseudospectrum equals the spectrum of the infinite Toeplitz operator, which is the Fourier transformation of its elements perpendicularly to the diagonal (see Appendix B 1 for the example of a tridiagonal matrix).
[40] A. Nahum, S. Vijay, and J. Haah, Operator spreading in random unitary circuits, Phys. Rev. X **8**, 021014 (2018).
[41] We can obtain a Markovian propagation of OTOC also following the procedures explained in [26]. However, the resulting transfer matrices in the latter approach are exponentially big in the system size, which makes it difficult to access large system sizes. The advantage of the Markov chain from [26] resides in the fact that it is possible to map circuits with nonrandom two-site gates and random one-site gates to a Markov chain; the Markov chain obtained from domain propagation can be obtained only for Haar random two-site gates.
[42] The given value for the phantom eigenvalue for BW PBC is exact because it coincides with the second largest eigenvalue for BW OBC, as well as with the decay of OTOC in infinite systems. The OTOC propagation in all three systems must be identical for times $t \sim n$ before the OTOC hits or "feels" the boundaries of the system.
[43] A. Bottcher and B. Silbermann, *Introduction to Large Truncated Toeplitz Matrices* (Springer, 1999).
[44] F. Diele and L. Lopez, The use of the factorization of five-diagonal matrices by tridiagonal Toeplitz matrices, Appl. Math. Lett. **11**, 61 (1998).
[45] A. M. Bruckner, J. B. Bruckner, and B. S. Thomson, *Real Analysis* (Prentice Hall, 1997).
[46] T. Koshy, *Catalan Numbers with Application* (Oxford University Press, 2008).
[47] R. P. Stanley, *Catalan Numbers* (Cambridge University Press, 2015).